

On the Numerical Prediction of the Influence of Tip Flow on Diffuser Stability

Bastian Drechsel, Joerg R. Seume, Florian Herbst

Institute of Turbomachinery and Fluid Dynamics
Leibniz Universität Hannover
Appelstr. 9,
30167 Hannover, Germany

Abstract

In previous studies, the pressure recovery of highly-loaded annular diffusers was identified to correlate with the Reynolds shear stresses at rotor outlet in the blade tip region. The origin and propagation of the Reynolds shear stresses, however, have not been experimentally clarified yet due to measurement probe constraints. Hence in the present work, the origin of these stresses, as well as the transport throughout the flow channel is analyzed by simulating the rotor with the scale adaptive turbulence model SAS-SST is used. Using the SAS approach, the Reynolds shear stress characteristics of the simulation are validated by the experimental results, whereas common RANS approaches are shown not to be appropriate. The tip leakage vortex is found to be the source of the Reynolds shear stress production. The interaction between vortex and mean flow leads to turbulent momentum transport. The Reynolds shear stresses propagate into the rotor far-field connected to the blade tip vortices which mix about four chord lengths downstream of the rotor trailing edge.

Keywords:

Tip leakage vortex, Reynolds shear stresses, scale adaptive simulation, diffuser

NOMENCLATURE

c	Velocity in stationary frame	[m/s]
c_p	Pressure recovery coefficient	[-]
k	Turbulent kinetic energy	[m ² /s ²]
L	Turbulent length scale	[m]
L_{VK}	Von Karman length scale	[m]
p	Static pressure	[Pa]
p_{tot}	Total pressure	[Pa]
r	Radial Direction	[-]
S	Scalar invariant of strain-rate tensor	[1/s]
u	Velocity tensor component	[m/s]
u	Rotational velocity in stationary frame	[m/s]
w	Relative Velocity in stationary frame	[m/s]
x	Axial direction in stationary frame	[-]

Greek symbols

α	Flow angle	[degree]
δ	Kronecker Delta	[-]
ζ	Pressure loss coefficient	[-]
ξ_2	Model constant	[-]
θ	Circumferential direction	[-]
θ	Circumferential angle	[degree]
κ	Isentropic exponent	[-]
λ	Stagger Angle	[degree]
μ	Dynamic viscosity	[kg/m s]
ρ	Density	[kg/m ³]

Abbreviations

CTA	Constant Temperature Anemometry
GCI	Grid Convergence Index
SAS	Scale adaptive simulation
TLV	Tip leakage vortex

Subscripts

in	Inlet
mod	modeled
out	Outlet
res	resolved
t	Turbulent
-	Average
,	Random fluctuation

Introduction

Exhaust diffusers downstream of steam or gas turbines are used to decelerate the turbine outflow. Caused by the area increase between inlet and outlet of the diffuser, the flow deceleration leads to a static pressure increase at the turbine outlet. Thus, more enthalpy can be transformed into technical work by the turbine at constant fuel consumption. As a parameter the pressure recovery coefficient

$$c_p = \frac{p_{out} - p_{in}}{p_{tot,in} - p_{in}} \quad (1)$$

describes the amount of kinetic energy at the diffuser inlet that is transferred into static pressure along the diffuser. The diffuser design follows empirical diffuser charts based on experimental studies of e.g. [1, 2] for different diffuser shapes and steady inflow conditions. These charts lead to rather long diffusers with small opening angles. Even if flow separation is avoided, the longer the diffuser

is the higher the total pressure losses are due to the comparably thicker boundary layer. Since the mentioned diffuser charts only take variations of homogeneous, axial inflow into account, these conditions differ largely from typical turbine outflows. Turbine outflows are inherently unsteady and incorporate swirl and inhomogeneous flow conditions due to tip leakage flows and wakes. These conditions were also found to affect the diffuser flow considerably [3–7]. Sieker and Seume [5] showed that highly turbulent, unsteady inflow can stabilize the flow field even if the diffuser was predicted to separate according to the diffuser charts. Kuschel and Seume [7] showed the impact of unsteady coherent vortices at the blade tips using unsteady hot-wire probes. Furthermore, they came to the conclusion that the Reynolds stresses of the rotor outflow at the blade tip are anisotropic. Based on these findings, Kuschel et al. [8] presented a correlation between the Reynolds shear stresses at the blade tip region of the rotor outflow and the pressure recovery in the two examined annular diffusers (see Fig. 1). They stated that the design of efficient diffusers requires taking the rotor outflow of the upstream located turbine stage into account.

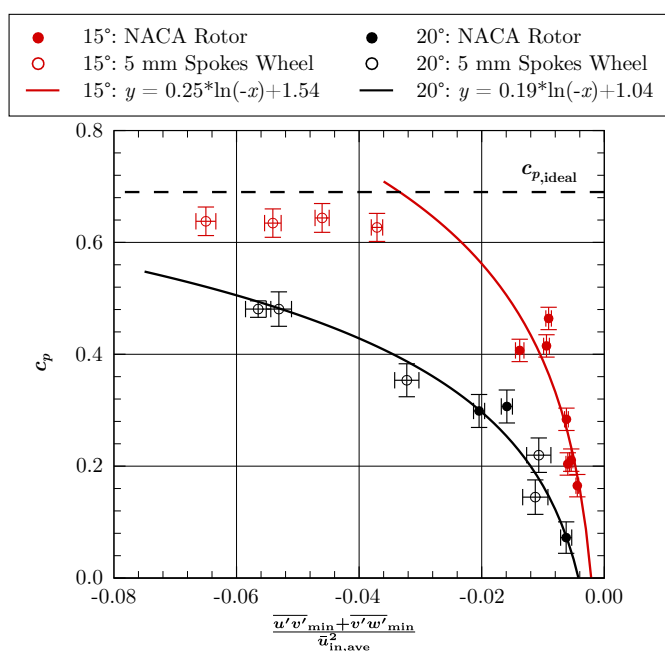


Fig.1: CORRELATION BETWEEN THE REYNOLDS SHEAR STRESSES OF THE ROTOR OUTFLOW AND THE PRESSURE RECOVERY OF THE ANNULAR DIFFUSER [8]

Drechsel et al. [9] performed scale-resolving simulations for an annular diffuser with a half cone opening angle of 15°, that is susceptible to flow separation. A rotor with symmetrical shaped blade is placed at the diffuser inlet. The chosen numerical approach uses the scale resolving SAS-SST turbulence model of [10] based on the SST-turbulence model. By resolving the turbulent flow scales, the anisotropic character of the flow is also resolved. It has been shown that the calculated Reynolds shear stresses and the resulting pressure recovery of the annular diffuser follow the correlation presented by [8].

The following study therefore bases on the numerical results of [9] and analyzes the propagation and origin of the Reynolds shear stresses at the rotor. Since the off-design operating point was found to lead to a higher pressure recovery of the annular diffuser, the focus is laid on this specific operating point. This will help to identify what kind of flow structures promote the stabilization of the diffuser’s boundary layer preventing it from flow separation, where this structures origin, and how they propagate in the flow field.

TEST FACILITY

The following experimental results used for the validation of the numerical approach were obtained using the low-speed diffuser test rig at the Institute of Turbomachinery and Fluid Dynamics (see Fig. 2). This rig is a 1/10 scale model of a heavy-duty gas turbine exhaust diffuser. The diffuser consists of an annular diffuser followed by a conical diffuser — this setup is typical for gas turbines. A wake generator is installed at the annular diffuser inlet. The wake generator is a single stage rotor without guide vanes that produces wake structures similar to those of turbomachines (Tab. 1). A detailed description of this rig can be found in [8] and [11]. For the experimental investigations the half-cone opening angle of the annular part was chosen to be 15°, and a NACA0020-profiled rotor with 30 blades was used as a wake generator.

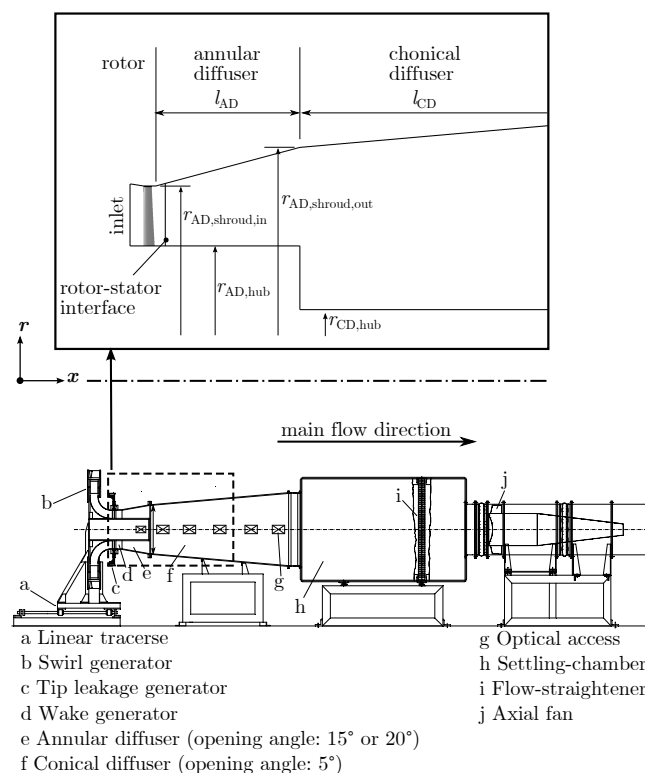


Fig.2: DIFFUSER TEST RIG

Hot-wire probes are used to determine the unsteady flow in the whole annular diffuser. The experiments were conducted using a DANTEC 55P91 3D hot-wire probe. This probe measures the unsteady velocity components in all three spatial directions with a temporal resolution of 50 kHz. It is connected to the DANTEC StreamLine frame with three anemometer modules (one for each wire) that operate in constant temperature mode (CTA). Kuschel [12] identified the measurement uncertainty of the CTA-probes with repeated measurements to be ±1 m/s.

To achieve statistical relevance, a large number of measurements had to be taken. These measurements were averaged using the Ensemble-Averaging approach. This approach, based on Taylor’s hypothesis splits the measurement data into a series of periodic data using a trigger signal. Each data series represents one blade passing. By averaging the periodic series, the unsteady flow’s signal can be decomposed into their periodic, deterministic contents and their stochastic contents. It was found that ensemble-averaging with 400 blade passings leads to good convergence of the flow statistics.

Numerical Method

All simulations in this paper were conducted with the commercial general-purpose solver ANSYS CFX 14.5 that provides a 2nd

Table 1: GEOMETRIC PROPERTIES OF THE TEST RIG

Rotor properties		Diffuser properties	
Shape	NACA0020	l_{AD}	235 mm
# of blades	30	l_{CD}	1735 mm
d_{hub}	280 mm	$r_{AD, hub}$	180 mm
h_{blade}	97 mm	$r_{AD, shroud, in}$	237 mm
$h_{tip, gap}$	1 mm	$r_{AD, shroud, out}$	300 mm
λ_{hub}	43°	$r_{CD, hub}$	35 mm
λ_{tip}	58°		

order discretization in time and space. The baseline turbulence model is the SST turbulence model by [13].

A more detailed simulation is achieved by the Scale-Adaptive Simulation (SAS) concept [10]. This model is based on the previously mentioned SST model, but includes a further blending function, which switches off the turbulence modeling depending on the timescale. This is realized by an additional term on the right hand side of the ω -transport equation reducing the turbulent viscosity μ_t , where the key part of this equation is the term

$$\tilde{\zeta}_2 \kappa S^2 \frac{L}{L_{vK}}, \quad (2)$$

based on the ratio of the model length scale L and the von Karman length scale L_{vK} . These values are significantly higher in the SAS regime than in the RANS regime. Whenever this happens, large structures in the main flow are spatially and temporally resolved, but within the boundary layer turbulence is still modeled. Therefore the SAS model is able to resolve turbulent mixing, and the prediction of anisotropic transport of shear stresses is much better than in RANS approaches. Viewed in an historical context, the SAS model is an improvement of the Detached-Eddy Simulation (DES) approach by [14], with lower sensitivity to grid resolution.

Ergorov and Menter [10] validated the SAS modification of the SST turbulence model for a series of applications Kluß et al. [6] showed the advantages of the SAS-SST model concerning the flow separation prediction of a highly loaded diffuser downstream of a single stage rotor.

Computational Model of the single stage rotor

As aforementioned, Drechsel et al. [9] showed numerically that the blade tip vortex pattern has a strong impact on the flow separation in a highly-loaded annular diffuser. These vortices are assumed to be the source of the Reynolds shear stresses that correlate with the pressure recovery in the annular diffuser [8]. In order to save computational time / effort, the diffuser section is not modeled as the focus is on the analysis of the rotor outflow. The correlation between Reynolds shear stresses and pressure recovery of the annular diffuser is already described by [8] and [12]. This setup allows to investigate the origin of the stresses but concerning the prediction of the propagation into the far-field (diffuser) limitations are expected. Thus, the validation can only be quantitative.

The numerical investigation of the rotor is conducted as follows: The rotor blades are shaped as NACA0020-profiles (Tab. 1). The numerical domain has a circumferential extent of one rotor passage. Preliminary numerical investigations showed no difference of the integral flow quantities for a domain extent of four, two, or one passage. Upstream of the rotor, the flow is guided from radial into the axial direction (see. Fig. 3). Downstream of the rotor, the numerical domain has an axial extent of 5.4 rotor blade chord lengths to ensure undistorted development of the blade tip vortices without any influence of the outlet boundary condition.

All solid walls are treated as viscous and fully turbulent, and automatic wall functions are applied. For the default mesh, the maximum y^+ -value was found to be 9.1 at the leading edge of the blade and about 3 at the shroud. At the intersection between the inlet section and the rotor domain, a stage interface was applied because the inflow of the rotor is circumferentially uniform. At domain inlet the

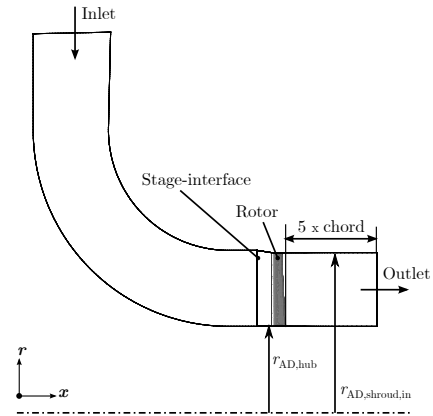


Fig.3: NUMERICAL DOMAIN

total pressure is equal to the ambient pressure 101 325 Pa at 15 °C. At the outlet a mass flow controller is used.

The rotor is investigated using an operating point with a rotational speed of 3000 min^{-1} and a mass flow of 5.5 kg s^{-1} , which is an off-design operating point of the rotor with overspeed. A tip leakage vortex forms due to the pressure difference between suction and pressure side of the blade.

All computations presented in this paper with the second-order upwind advection scheme reached convergence for momentum and turbulence quantities with maximum residuals below 1×10^{-3} and RMS residuals below 3×10^{-5} . Calculations with the blended central difference scheme showed maximum residuals below 8×10^{-2} and RMS residuals below 2×10^{-4} . With both advection schemes imbalances of massflow and energy below $10^{-6}\%$ were reached. In all time-resolved computations, at least one complete flow through the computational domain and five rotations of the rotor are simulated before statistical quantities are evaluated. For the unsteady simulation the time step size is $1 \times 10^{-6} \text{ s}$ which corresponds to 667 samples per blade passage.

Grid convergence study

All numerical simulations are susceptible to various errors [15]. In order to estimate the error resulting from the numerical grid, a grid convergence study is conducted for steady RANS simulations with the SST turbulence model. In this study the baseline grid (see. Fig. 4), as well as two additional grids (one coarse and one refined) are investigated through the total pressure loss coefficient

$$\zeta = \frac{P_{tot, in} - P_{tot, out}}{P_{tot, in} - P_{in}} \quad (3)$$

that correlates with the quality of the numerical simulation of the turbulence. Additionally, the effect of the outflow angle at rotor outlet is analyzed. The results show good convergence for both parameters.

It can be seen that even with the medium-fine grid the discretization error is comparably small. When focusing on the main flow even the coarse grid seems to be appropriate. Nevertheless, the GCI-values for the tip flow region (span 90...100%) show larger errors for the coarser meshes. Indeed, the error can be reduced using a finer grid but as computational costs increase dramatically with the number of grid points, the best trade-off between accuracy and computational costs can be achieved with the medium-fine grid. A grid convergence study concerning the time step size was not conducted.

Analysis of the rotor flow field

To validate the SAS approach, first numerical results are compared to experimental hot-wire measurements at 50% span. As the SAS turbulence model has been shown to be appropriate, it follows that a 2d analysis of the flow in the blade tip region at 97% span is

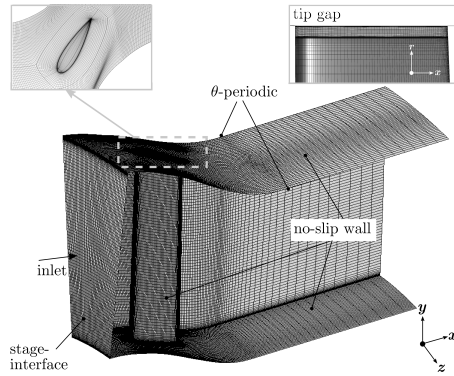


Fig.4: COMPUTATIONAL MESH AND BOUNDARY CONDITIONS OF THE SINGLE STAGE NACA-PROFLED ROTOR, INLET DUCT NOT SHOWN

Table 2: GRID CONVERGENCE INDEXES OF ζ AND OF α WITH AN ASSUMED CONSERVATIVE EXTRAPO- LATION ORDER OF $p = 1$ AND A SAFETY FACTOR OF $F_s = 1.25$ [15] FOR RANS-SST SIMULATIONS

Cells per passage	GCI_ζ	$GCI_{\zeta,Tip}$	GCI_α	$GCI_{\alpha,Tip}$
1.1 M	1.03%	6.56%	0.25%	2.27%
1.8 M	0.6%	4.13%	0.14%	1.25%
8.1 M	0.36%	2.53%	0.089%	0.76%

a good choice as the basis for the detailed investigation of the blade tip vortices and the resulting Reynolds shear stresses.

2d flow analysis of the rotor outflow at midspan

In Fig. 5 the simulated wake profile at midspan are compared to the results of hot-wire measurements by [12].

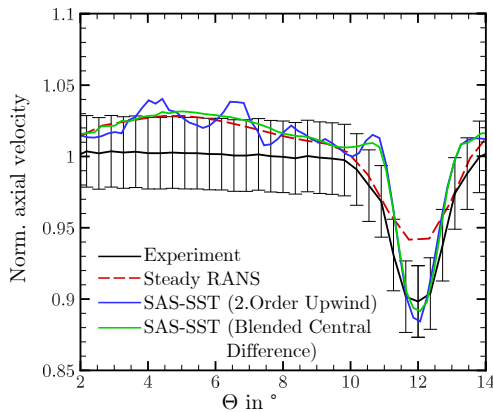


Fig.5: WAKE VELOCITY PROFILES 1.33 CHORD LENGTH DOWNSTREAM OF ROTOR AT 50% SPAN

First, the flow field at 50% span is analyzed 1.33 chord length downstream of the rotor. Here the flow is two dimensional. Note, the deviating characteristics of the SAS calculation caused by the different advection schemes (2.Order Upwind and Blended Central Differences) will be discussed further below. Comparing the experimental results with the numerical simulations, it can be seen that the experiments and the SAS simulation show good agreement. In contrast, the RANS simulations calculate the wake region to have a wider than expected circumferential extent, as well as an insufficient relative wake deficit.

Hence, in Fig. 6 a) the difference of the absolute axial velocity between the RANS simulation and the SAS simulation is shown.

This helps to understand the origin of the wake difference for the two numerical approaches. Both different simulation of the boundary layer at the rotor surface and deviant turbulent mixing downstream of the rotor could lead to the wake profile difference.

Both calculations show an identical flow field from the inlet to approximately 0.63 chord length of the blade. Starting from 0.63 chord length at the suction side of the blade, the axial velocity in the boundary layer calculation is higher for the RANS calculation compared to that of the SAS simulation. Downstream of the trailing edge, the axial velocity is relatively high for the RANS simulation, indicated by a negative axial velocity difference in the wake core flow. Nevertheless, the velocity gradient is low, such that the circumferential extent of the wake is larger for the RANS. Hence, the axial velocity difference between RANS and SAS is positive outside of the wake core.

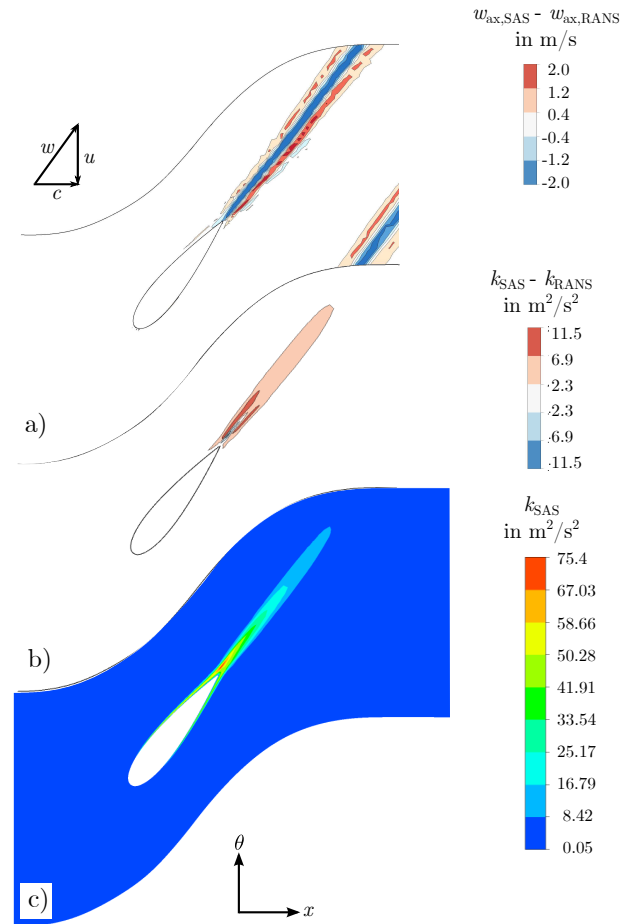


Fig.6: FLOW FIELD COMPARISON OF SAS AND RANS AT 50% SPAN
a) AXIAL VELOCITY DIFFERENCE , b) TURBULENT KINETIC ENERGY DIFFERENCE, c) TURBULENT KINETIC ENERGY OF SAS

To conclude, the wake profile of the unsteady calculation clearly shows better agreement with the experiments. Both the velocity gradient and the relative wake deficit match very well with the experimental result, even if the wake is slightly small indicating insufficient mixing.

Under the assumption that turbulent stresses promote turbulent mixing, the turbulent kinetic energy

$$k = \frac{\overline{u'_i u'_i}}{2} \tag{4}$$

provides information on the turbulent mixing in the flow field.

While the shear stresses of the RANS simulations are calculated following the Boussinesq hypothesis

$$\overline{u'_i u'_j}_{\text{mod}} = -\frac{\mu_t}{\rho} \left(\frac{\partial \bar{u}_i}{\partial x_j} + \frac{\partial \bar{u}_j}{\partial x_i} \right) - \frac{2}{3} \rho k \delta_{ij} \quad , \quad (5)$$

the Reynolds shear stresses of the SAS simulation

$$\overline{u'_i u'_j}_{\text{SAS}} = \overline{u'_i u'_j}_{\text{res}} + \overline{u'_i u'_j}_{\text{mod}} \quad (6)$$

are the sum of the resolved stresses by the SAS term and the modeled turbulence (k -term). The resolved stresses include solely statistical variations, whereas the stresses derived from the Boussinesq-hypothesis includes both deterministic and stochastic stresses (as long as they are not resolved by the SAS approach).

In Fig. 6 b) the difference in turbulent kinetic energy between the scale adaptive approach and the RANS-simulation is shown. This corresponds to the development of the wake structures that were analyzed above. A difference between both models is observable from approx. 0.63 chord length on. Here the scale adaptive simulation shows a higher level of turbulent kinetic energy in the wake region. This confirms the slower turbulent decay of the turbulent energy that was also detected by Drechsel et al. [9]. As a result, due to the faster decay of the turbulent kinetic energy the wake widens faster, too, in case of the steady RANS. Taking into account the turbulent kinetic energy of the SAS simulation (Fig. 6 c)), it can be concluded that the production of k is similar for RANS and SAS upstream of the blade and along the blade up to approx. 66% span. Nevertheless differences occur in the wake of the blade. Here the SAS simulation shows a clearly slower decay in the wake region compared to the RANS simulation.

The turbulent kinetic energy presented in Fig. 7 provides a comparison of the TKE development for a blade passing. The experimental measured TKE is the highest followed by the SAS and the RANS simulation. It can be concluded that the input of turbulent quantities into the diffuser for both numerical approaches is less than in the real flow, even if the SAS shows advantages.

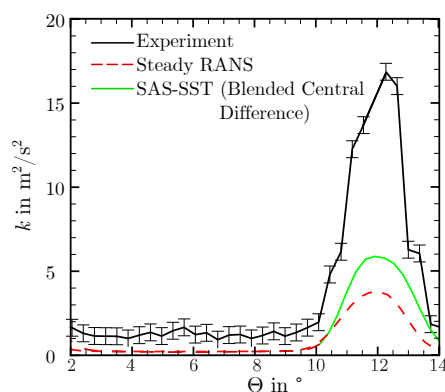


Fig.7: TKE PROFILES 1.33 CHORD LENGTH DOWNSTREAM OF ROTOR AT 50% SPAN

In Fig. 8 the Reynolds shear stresses are shown for one blade passing. The magnitudes of the stresses in the radial-axial, and radial-circumferential direction are of similar magnitude, whereas the stresses in the axial-circumferential direction are clearly higher. This behavior can be explained by the flow propagating in axial direction and the rotation of the rotor in the circumferential direction. This leads to high Reynolds shear stresses in the mentioned direction due to the wake propagation. The agreement between experiments and simulation is acceptable taking into account that the mesh in the core region is relatively coarse so only few scales of the turbulence field are resolved by the SAS approach. Using the Lumley-charts [16] to characterize the turbulence (details see

Kuschel et al. [8]), the turbulence was found being in good accordance to the experiments (see. Fig. 9). Both experiment, and numerical simulation show an axisymmetric turbulence with higher third component. This leads to the conclusion that the scale adaptive approach is able to model the anisotropic characteristics of the flow field.

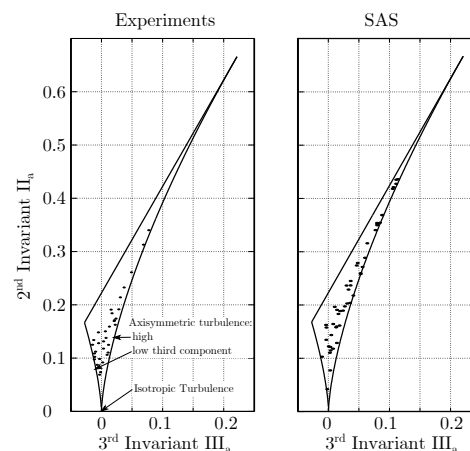


Fig.9: LUMLEY-CHARTS OF THE REYNOLDS SHEAR STRESSES 1.33 CHORD DOWNSTREAM OF THE ROTOR AT 50% SPAN

Effect of the numerical advection scheme on the SAS simulation

In Fig. 5 it can also be seen, that different wake profiles were calculated depending on the advection scheme that was used. Wiggles are observable between two wakes for the high resolution scheme of ANSYS CFX in the mean flow. These are not connected to any turbulent structures, and therefore they were identified as being non-physical. The mentioned wiggles can be traced back to the trailing edge at blade tip. Here the flow values show high gradients that were identified as causing the mentioned effect in combination with the advection scheme.

The high resolution advection ANSYS CFX scheme is a second-order upwind differencing scheme, which is more accurate in terms of reproducing steep spatial gradients compared to first-order differencing schemes [17]. Strelets [18] pointed out that less-dissipative centered schemes are more convenient for regions where the LES term of the SAS is active, whereas the upwind schemes leads to better results in the case where the SAS works in RANS mode. Nevertheless, even the upwind scheme results in acceptable accuracy if the grid is fine enough, but in general this leads to very fine meshes and correspondingly high computational costs. Therefore, the upwind scheme was found to be appropriate only when the numerical diffusion is significantly less than the physical diffusion [19]. As a result, Strelets [18] proposed the combination of a first order upwind scheme and a central difference scheme with a blending factor to switch between the two. Consequently, the use of the bounded central difference scheme in ANSYS CFX leads to better results in the unsteady simulation with the SAS-SST turbulence model. Here the so called bounded central difference scheme is used. This scheme has a blending factor that switches to the first-order upwind scheme whenever the central difference scheme leads to non-physical oscillations [20].

The numerical simulation using the bounded central difference scheme looks very promising with regards to the wake profiles in Fig. 5. Here only minor wiggles are observable. Still at the suction side flank of the wake, a single overshoot remains, but its influence on the mean flow is negligible.

2-D analysis of the flow at blade tip

Above it was shown that the SAS approach matches the experiments at 50% rotor span very well, where the flow is rather two

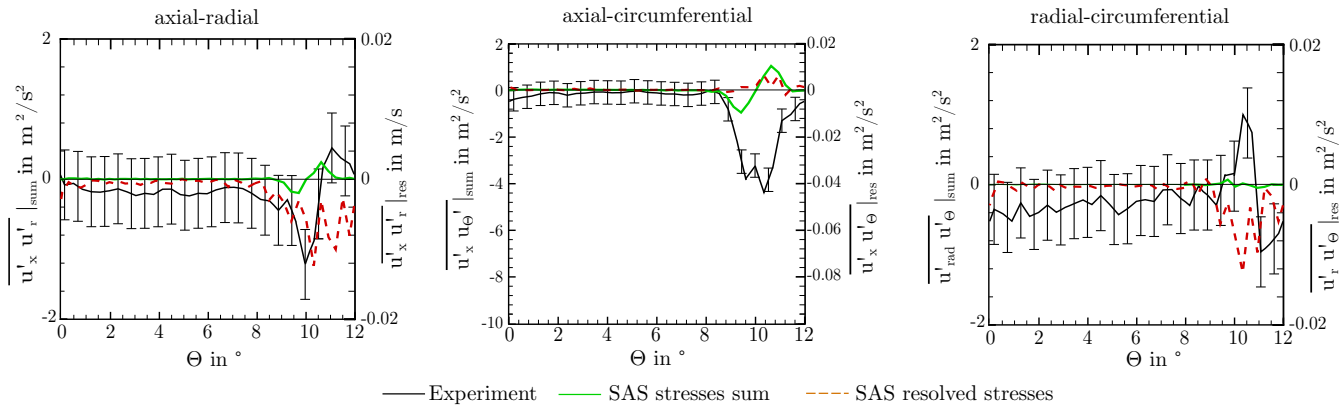


Fig.8: REYNOLDS SHEAR STRESSES 1.33 CHORD LENGTH DOWNSTREAM OF ROTOR AT 50% SPAN

dimensional. Hence, the following paragraph focuses on the rotor outflow at the blade tip, where the tip leakage flow causes complex vortices which can lead to a three dimensional flow field. Complementary to the aforementioned analysis, Fig. 10 shows the wake profile at 97% span. This position is equal to the highest measuring position, since the probe size allows no hot-wire measurements closer to the wall.

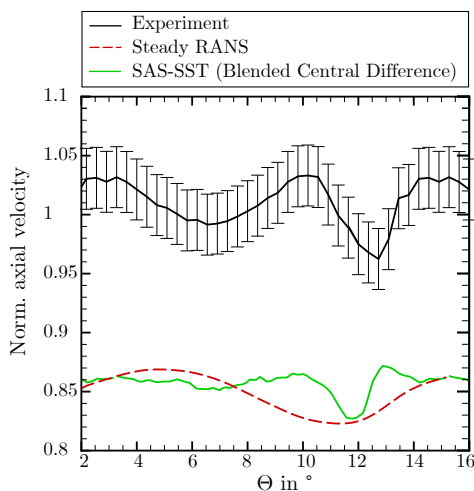


Fig.10: WAKE VELOCITY PROFILES 1.33 CHORD LENGTH DOWNSTREAM OF ROTOR AT 97% SPAN EVERY THIRD ERROR BAR SHOWN

The experimental results show that the wake is insignificantly deflected in circumferential direction compared to the wake at 50% span. Next to the wake, at approximately half a blade passing, a second velocity deficit is detectable. Here the blade tip vortex of the adjacent blade passes, which will be discussed further below. While the RANS simulation does not match the characteristics of the experimental results, the SAS does. Disregarding the offset between the experiment and the SAS simulation, it is good to see that the SAS fits both the relative velocity deficit of the wake as well as that of the blade tip vortex. Even the circumferential extent of the wake is similar.

The offset between experiment and simulation is due to the deviant shroud contour. As previously mentioned, the radius of the shroud is constant in the numerical domain. In contrast to the numeric domain in the experimental setup, the rotor is followed by the diffuser. The diffuser's inlet is located 0.33 of chord length downstream of the rotor, so that the position mentioned in Fig. 10 is downstream of the diffuser inlet. Hence, in the experiments the an-

alyzed position is outside of the boundary layer, whereas it is within for the numerical investigation. Still, concerning the propagation of the blade tip vortices numerical simulation and experiment are comparable at this position because the vortices were found to propagate rather axial into the diffuser [9]. Since the focus of this work is put on the analysis of the turbulent quantities that are connected to the vortex structures, no adjustment of the radial measurement position for the analysis of the velocity profile was made. But it has to be kept in mind, that downstream of 0.3 chord of the blade, the frictional effects at the wall near region increase for the numerical setup.

Characterization of Reynolds shear stresses in blade tip region

Kuschel [12] identified the Reynolds shear stresses as having major impact on the flow's stability in highly loaded diffusers and observed that the stresses were anisotropic. Therefore he assumed that a turbulence model should be used that provides the anisotropic simulation of the Reynolds shear stresses, like the SAS-SST turbulence model.

In Fig. 11 the wake profile 0.33 chord length downstream of the blade's trailing edge is shown. Concerning the position of the wake ($\theta \approx 1...3^\circ$), a slightly offset in circumferential direction is detectable which indicates the overturning of the flow being higher for the experiments. Furthermore, it can be seen that the circumferential distance between wake and tip leakage vortex ($\theta \approx 10...12^\circ$) is higher for the experiments that is assumed to occur due to the higher overturning.

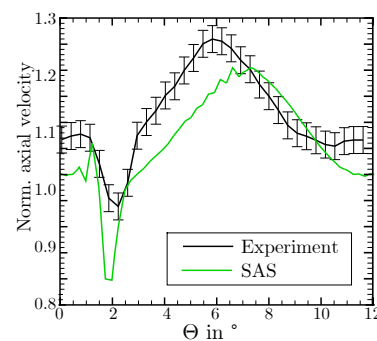


Fig.11: WAKE VELOCITY PROFILES 0.33 CHORD LENGTH DOWNSTREAM OF ROTOR AT 97% SPAN

Concerning the Reynolds shear stresses (see Fig. 12), an insufficient magnitude of the Reynolds shear stresses of the simulation is observable. Furthermore, the trend of the modeled stresses is not in accordance with the experiments. Since the analysis of the numeri-

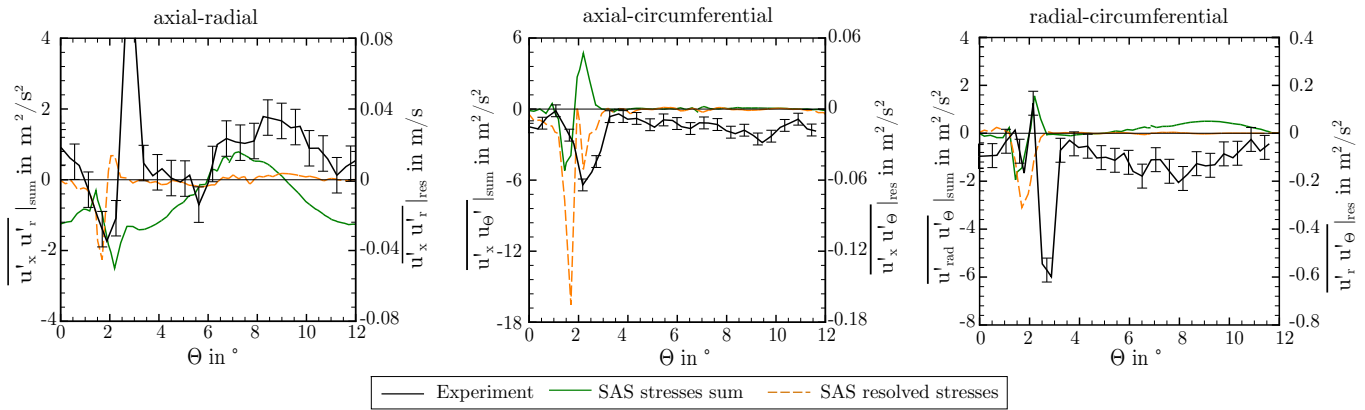


Fig.12: REYNOLDS SHEAR STRESSES 0.33 CHORD LENGTH DOWNSTREAM OF ROTOR AT 97% SPAN EVERY THIRD ERROR BAR SHOWN

cal results was conducted in the rotating frame of reference, both the modeled stresses, and the resolved stresses are calculated excluding the deterministic fluctuations in terms of e.g. wakes. The deviation thus occurs clearly in the stochastic fluctuations modeled by the k -term. Hence, it can be concluded that the simulation allows the identification regions, where the Reynolds shear stress are significant but an exact prediction of the stresses' magnitude is not given. Furthermore, in future studies the amount of resolved structures has to be improved by refining the grid and/or increasing the temporal resolution in order to derive a better prediction of the absolute values of the calculated stresses. Concerning the characteristics of the turbulence, the Lumley-charts in Fig. 13 indicate a axi-symmetrical turbulence of the resolved stresses which is in accordance with the experiments [8]. Compared to the turbulence characteristic in the mean flow (Fig. 9) it can be seen that the data points show clearly a tendency for axi-symmetrical turbulence with high third component.

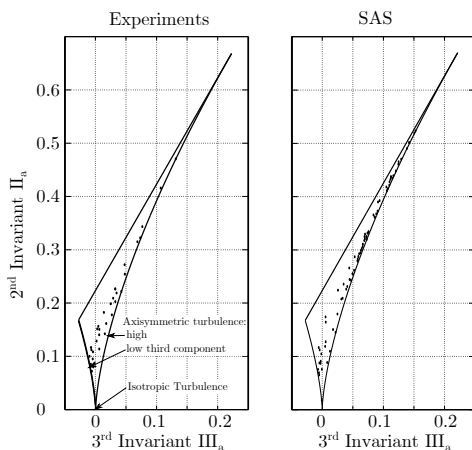


Fig.13: LUMLEY-CHARTS OF THE REYNOLDS SHEAR STRESSES 33% CHORD DOWNSTREAM OF THE ROTOR AT 97% SPAN

In order to identify the advantages of the scale adaptive approach compared to the RANS-simulation in Fig.14 the Reynolds shear stresses in radial-circumferential direction are presented for the steady and unsteady RANS-simulation with the SST turbulence model, and the SAS-SST simulation. It can be seen that the modeled stresses of RANS and URANS simulation are nearly identical. On the other side the SAS-SST simulation deviates significantly in the wake region ($\theta \approx 6...9^\circ$). Here both the minimal and maximal val-

ues are clearly higher (approx. one order) compared to the RANS and URANS simulation. Compared to the experimental results from [9] it can be stated that the profile of the Reynolds stresses agrees for the scale adaptive simulation whereas it is not captured by the RANS approach.

Therefore, it can be concluded that the SAS-SST model is advantageous in terms of momentum transport into the boundary layer caused by vortex structures that is driven by the shear stresses in radial direction [12]. Furthermore, it was shown that even if the modeled stresses of the SAS-SST turbulence model differ from the experiments, the results of scale-adaptive approach matched the experiments better compared to the RANS.

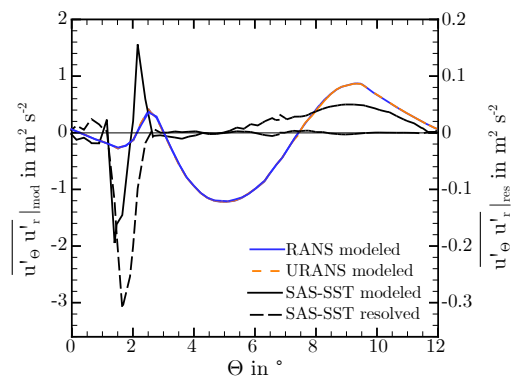


Fig.14: SHEAR STRESSES IN CIRCUMFERENTIAL-RADIAL DIRECTION OF DIFFERENT NUMERICAL APPROACHES, 0.33 CHORD DOWNSTREAM OF THE ROTOR, 97% SPAN

Circumferentially averaged Reynolds shear stresses

The following paragraph will show the identification process of where the experimentally-observed Reynolds shear stresses originate and how they propagate. Due to the probe size, this has not yet been experimentally clarified. In a first step the origin of the stresses will be identified by analyzing the resolved stresses. Fig. 15 shows the circumferential average of the absolute Reynolds shear stresses. In order to focus on the significant areas, the flow channel is not shown completely. In total, three spots of significantly high Reynolds shear stresses can be identified. The highest average occurs at the leading edge of the blade. Here a separation vortex forms since boundary layer at the casing is thin compared to the gap size. So the flow can enter the gap but separates at the leading edge due

to the high flow deviation.

Drechsel et al. [9] showed that here at blade tip a separation vortex forms that propagates into the blade tip gap resulting in high Reynolds shear stresses. The other two spots are situated at 0.7 chord of the blade in the blade tip gap and close to the trailing edge at the blade tip.

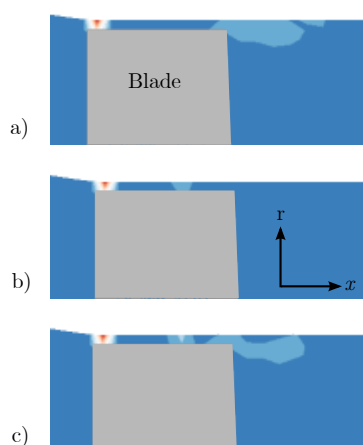


Fig.15: CIRCUMFERENTIAL AVERAGED ABSOLUTE REYNOLDS SHEAR STRESSES; SPAN 0.9 ... 1, DARK BLUE: STRESSES ≈ 0
A) AXIAL-RADIAL, B) AXIAL-CIRCUMFERENTIAL, B) RADIAL-CIRCUMFERENTIAL

The analysis of the averaged-absolute shear stresses gives a good impression of where the stresses originate in the flow field i.g. where the following analysis has to focus on. Since the above presented results neither contain any information about the direction of the stresses nor the circumferential position of high stresses, this also has to be studied. Recalling that Kuschel [12] showed the correlation of the Reynolds shear stresses with a high negative radial component and the pressure recovery in highly-loaded diffusers, at least the direction of the stresses is very important. On the other hand, identifying the circumferential origin of the stresses helps to design rotor blades that stabilize highly-loaded diffusers due to their turbulent outflow characteristics.

Origin and propagation of Reynolds shear stresses

In Fig. 16 two pitches of the rotor are shown. For the first pitch, the Reynolds shear stresses in radial-circumferential direction are plotted as an example. This component was found to give a good representation of the flow, especially concerning the shear stress spots in the blade tip region (see. Fig. 15). For the second pitch, the vortices are presented using the λ_2 -Criterion. The vortices are plotted for an eigenvalue of $-6.86 \times 10^6 \text{ s}^{-2}$ and colored according to streamwise vorticity. It can be seen that the level of shear stresses at the channel inlet is negligible, whereas the first spot of high shear stresses is observable at suction side at the rear part of the blade (Fig. 16 ①). From the comparison of this region with the blade tip vortices, it can be assumed that the high Reynolds stresses are due to the separation of the tip leakage vortex at the blade tip. From here the shear stresses propagate downstream with the tip leakage vortex. Note that the flow angle of the blade tip vortex is higher than the flow angle of the main flow. This overturning is caused by the momentum of the tip flow, as described by Willinger and Hasselbacher [21]. In the experiments, the inlet of the diffuser is located about 0.5 of axial chord length downstream of the rotor, where the Reynolds shear stresses were found to influence the boundary layer, therefore in the following paragraph the focus is on the propagation of the stresses downstream of the rotor. Further downstream of the rotor, regions with distinctive region of high stresses can clearly be seen (both positive and negative). These regions are connected

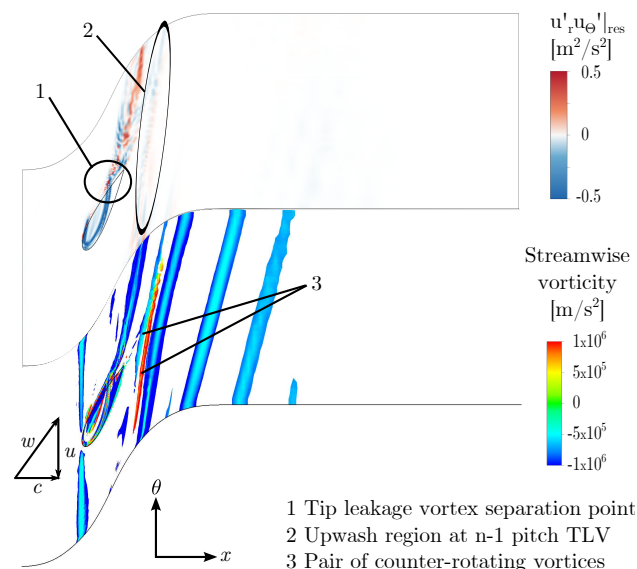


Fig.16: PROPAGATION OF REYNOLDS SHEAR STRESSES DOWNSTREAM OF ROTOR, 99% SPAN

to the tip leakage vortices. Therefore as the vortices dissipate, the stresses decay. Approximately four axial chord lengths downstream of the rotor the tip leakage vortices are mixed out and the Reynolds shear stresses reach the final state with a magnitude in the order of 1×10^{-2} . So the region of influence of the Reynolds shear stresses is clearly less compared to the extent of the blade tip vortices. The extent of the Reynolds shear stresses in axial direction is comparable to the results of Lakshminarayana and Reynolds [22] in the wake region at midspan.

Even if the first appearance of the Reynolds shear stresses was identified to be at the separation point of the tip leakage vortex at the blade, it is notable that the maximum values occurs further downstream at the blade vortex of the previous blade at the upstream vortex side (Fig. 16 ②). Here both the maximum and minimum values of the stresses can be found. In order to understand the mechanisms that lead to an increase in Reynolds shear stresses close to the tip leakage vortex, the interaction between vortex and the flow near the casing has to be analyzed in more detail. This will help to understand both the occurrence of such high Reynolds shear stresses at tip leakage vortex regions, and the maximum stress values at the TLV of the previous blade passing.

Consider the flow region between the tip leakage vortex of the current pitch (pitch n) and that of pitch n-1 is discussed (see Fig. 17): As described in Drechsel et al. [9], the transport of free stream fluid towards the casing boundary layer is mainly driven by the rotation of the tip leakage vortex. At the downstream side of the vortex the fluid is pulled towards the casing, whereas at the upstream side of the vortex the fluid is pushed towards the mean flow, as the tip leakage vortex is rotating counter-clockwise in the stream-wise direction. Nevertheless, in Fig. 16 at the upstream region of the n-1 vortex, two counter-rotating smaller vortices are indicated by the λ_2 -Criterion. Here the mean flow is transported with high momentum into the casing region resulting in negative Reynolds stresses [8]. Since the flow angle of the tip leakage vortex and the mean flow differ, the flow is deflected by the TLV towards the mean flow with a high negative radial velocity component and as such the Reynolds shear stresses with a radial component show a maximum. Analyzing the streamlines in that region leads to the conclusion that the two smaller vortex regions in the upstream region of the n-1 TLV are not distinctive vortices. Even if the flow has a high vorticity due to the high deflection of the flow, no vortices form in the conventional manner. A further result of the interaction between mean flow and TLV is the deflection of the TLV in axial direction, such that the

flow angle of the vortex decreases during its propagation.

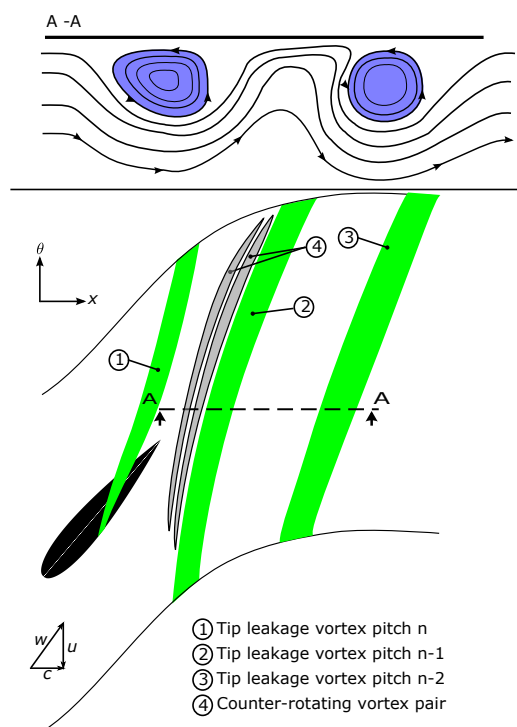


Fig.17: SKETCH OF THE TIP LEAKAGE VORTICES AND THE RESULTING COUNTER-ROTATING VORTEX PAIR INDICATED BY THE λ_2 -CRITERION

In the region between the TLV of pitch $n-1$ and $n-2$, the peak values of the Reynolds shear stresses are comparable smaller to that discussed previously. Since both the strength of the vortices due to the turbulent mixing, and the flow angle difference between vortex and mean flow is decreased, the momentum transport into the casing region decreases as well. This leads to smaller Reynolds shear stresses in the radial direction. The previous observations leads to the conclusion, that both powerful tip leakage vortices and a high underturning or overturning of the TLV compared to the mean flow provoke Reynolds shear stresses with high radial component in the casing region.

Conclusions

Numerical scale-resolving simulations (SAS-SST turbulence model) of a NACA-profiled rotor at off-design operating point were conducted and the prediction of the tip leakage vortex and the Reynolds shear stresses of the near-casing flow field were analyzed.

The qualitatively validation by means of the simulation of the rotor outflow without a diffuser further downstream against hot-wire measurements in the diffuser test rig showed the advantages of the scale-resolving simulation concerning the simulation of the turbulent quantities compared to the steady RANS-simulation. The calculated Reynolds stresses of the SAS-SST model qualitatively match the characteristics of the experimental values, whereas the steady RANS and unsteady RANS with the SST turbulence model do not. One reason was found in the propagation of the turbulent kinetic energy into the near-field of the rotor outflow. While both numerical approaches calculate the same turbulent quantities upstream of the blade and along approximately 60% of the blade chord, in the wake a difference is observable between the two models. Here, the turbulent kinetic energy of the RANS-simulation decays much faster, so the RANS approach shows lower turbulent quantities in the far-field, compared to the experiments and the SAS

approach. This strongly effects the flow in the flow channel further downstream as for example the flow development in a diffuser.

Analyzing the flow in the blade tip region, three sources of Reynolds shear stresses were identified. First, at the leading edge of the rotor due to the blade tip separation vortex. Secondly, at the suction side of the blade at the separation point of the tip leakage vortex. Thirdly, downstream of the trailing edge in the near-wall region. Here, the interaction between mean flow and tip leakage vortex was found to act as source of the Reynolds stresses. Furthermore, the analysis of the flow leads to the assumption that high Reynolds shear stresses are promoted via a high flow angle difference between mean flow angle and tip leakage vortex.

Future numerical investigations should focus on the improved simulation of resolved turbulent structures. They were found to be still significantly less compared to the modeled stresses. Therefore, further investigations on both grid and temporal resolution would be promising avenues of research. Furthermore, the flow field of the turbine stages has to be analyzed in order to clarify whether the deviation of the flow angle between mean flow and tip leakage flow is similar to that of the single stage rotor of the diffuser test rig. This supports both, the assumption that the rotor generates wakes are similar to real turbomachines and that the stabilization of the diffuser is also possible with a real turbine located upstream.

Acknowledgments

The investigations were conducted as part of the joint research program COORETEC-Turbo 2020 in the frame of AG Turbo. The work was supported by the Bundesministerium für Wirtschaft und Technologie (BMWi) as per resolution of the German Federal Parliament under grant number 03ET2011I and MAN Diesel & Turbo. Furthermore, the authors thank AG Turbo and MAN Diesel & Turbo for the permission to publish this work, and ANSYS for providing CFX in an academic license. Last but not least, the authors thank the Leibniz Universität Hannover IT Services (LUIS) for the computational resources provided. The responsibility for the content lies solely with its authors.

References

- [1] Sovran, G., and Klomp, D., 1967. "Experimentally determined Optimum Geometries for Rectilinear Diffusers with Rectangular Conical or Annular Cross-Section". *Fluid mechanics of internal flow : Proceedings of the Symposium on the Fluid Mechanics of Internal Flow, General Motors Research Laboratories, Warren, Michigan*.
- [2] ESDU, 1990. *Introduction to Design and Performance Data for Diffusers*. London.
- [3] Barker, A. G., and Carrotte, J. F., 2001. "Influence of Compressor Exit Conditions on Combustor Annular Diffusers Part II: Flow Redistribution". *Journal of Propulsion and Power*, **17**(3), pp. 687–694.
- [4] Sieker, O., and Seume, J. R., 2008. "Influence of Rotating Wakes on Separation in Turbine Exhaust Diffusers". *Journal of Thermal Science*, **17**(1), pp. 42–49.
- [5] Sieker, O., and Seume, J. R., 2008. "Effects of Rotating Blade Wakes on Separation and Pressure Recovery in Turbine Exhaust Diffusers". *Proc. ASME Turbo Expo 2008, June 9-13, Berlin, Germany*.
- [6] Kluß, D., Stoff, H., and Wiedermann, A., 2009. "Effect of Wakes and Secondary Flow on Re-attachment of Turbine Exit Annular Diffuser Flow". *Journal of Turbomachinery*, **131**(4), pp. 1–12.
- [7] Kuschel, M., and Seume, J., 2011. "Influence of Unsteady Turbine Flow on the Performance of an Exhaust Diffuser".

- Proc. ASME Turbo Expo 2011, June 6-10, Vancouver, Canada.*
- [8] Kuschel, M., Drechsel, B., Kluß, D., and Seume J. R., 2015. "Influence of Turbulent Flow Characteristics and Coherent Vortices on the Pressure Recovery of Annular Diffuser, Part A: Experimental Results". *Proc. ASME Turbo Expo 2015, June 15-19, Montreal, Canada.*
- [9] Drechsel, B., Müller, C., Herbst, F., and Seume J. R., 2015. "Influence of Turbulent Flow Characteristics and Coherent Vortices on the Pressure Recovery of Annular Diffuser, Part B: Scale-Resolving Simulations". *Proc. ASME Turbo Expo 2015, June 15-19, Montreal, Canada.*
- [10] Egorov, Y., and Menter, F., 2008. "Development and Application of SST-SAS Turbulence Model in the DESIDER Project". In *Advances in Hybrid RANS-LES Modelling*, S.-H. Peng and W. Haase, eds., Vol. 97 of *Notes on Numerical Fluid Mechanics and Multidisciplinary Design*. Springer Berlin Heidelberg, Berlin and Heidelberg, pp. 261–270.
- [11] Fleige, H.-U., and Riess, W., 2001. "Investigations of Gas Turbine Exhaust Diffuser Flows". *Proc. of the 4th European Conference on Turbomachinery, Florence, Italy*, pp. 665–674.
- [12] Kuschel, M., 2014. "Einfluss von Sekundärströmungen auf den Druckrückgewinn in Axialdiffusoren (Influence of the Secondary Flow on the Pressure Recovery in Annular Diffusers)". *Berichte aus dem Institut für Turbomaschinen und Fluid-Dynamik*, 3.
- [13] Menter, F. R., 1994. "Two-equation eddy-viscosity turbulence models for engineering applications". *AIAA Journal of Fluids Engineering*, 38(8), pp. 269–289.
- [14] Spalart, P. R., 2000. "Strategies for turbulence modelling and simulations". *Int. J. Heat Fluid Flow*(21), pp. 252–263.
- [15] Committee, A. V. & V. ., 2009. "Standard for Verification and Validation in Computational Fluid Dynamics and Heat Transfer". *The American Society of Mechanical Engineers*, pp. 213–228.
- [16] Lumley, J. L., and Newman, G. R., 1977. "Return of Isotropy of Homogeneous Turbulence". *Journal of Fluid Mechanics*, 82(pt 1), pp. 161–178.
- [17] ANSYS CFX, 2013. "CFX-Solver Theory Guide, Release 15.0".
- [18] Strelets, M., 2001. "Detached Eddy Simulation of Massively Separated Flows". *39rd AIAA Aerospace Sciences Meeting and Exhibit, January 8-11, Reno, Nevada, USA.*
- [19] Gresho, P. M., and Lee, R. L., 1981. "Don't suppress the wiggles—They're telling you something!". *Computers & Fluids*, 9(2), pp. 223–253.
- [20] Jasak, H., Weller, H. G., and Gosman, A. D., 1999. "High resolution NVD differencing scheme for arbitrarily unstructured meshes". *International Journal for Numerical Methods in Fluids*, 31(2), pp. 431–449.
- [21] Willinger, R., and Haselbacher, H., 1998. "The Role of Rotor Tip Clearance on the Aerodynamic Interaction of a Last Gas Turbine Stage and an Exhaust Diffuser". *Proc. ASME International Gas Turbine and Aeroengine Congress and Exhibition 1998, June 2-5, Stockholm, Sweden.*
- [22] Lakshminarayana, B., and Reynolds, B., 1979. "Turbulence Characteristics in the Near Wake of a Compressor Rotor Blade". *AIAA Journal*, 18(11), pp. 1354–1361.